

# The Influence of Brittleness of Interlayers on the Failure Behavior of Bedding Rock; Experimental Test and Particle Flow Code Simulation

Rahim Mortezaei<sup>1</sup>, Seyed Davoud Mohammadi<sup>1\*</sup>, Vahab Sarfarazi<sup>2</sup>, Reza Bahrami<sup>3</sup>

<sup>1</sup> Department of Geology, Bu-Ali Sina University, Mahdieh Ave., P.O.B. 6517538695, Hamedan, Iran

<sup>2</sup> Department of Mining Engineering, Hamedan University of Technology, Mardom St., P.O.B. 65155579, Hamedan, Iran

<sup>3</sup> Department of Civil Engineering, Islamic Azad University (Beyza Branch), P.O.B. 7363111341, Beyza, Iran

\* Corresponding author, e-mail: [d.mohammadi@basu.ac.ir](mailto:d.mohammadi@basu.ac.ir)

Received: 19 July 2023, Accepted: 16 August 2023, Published online: 18 September 2023

## Abstract

In the present study, the effects of angle and brittleness of interlayers on the shear failure behavior of notched bedding rock have been scrutinized using experimental shear tests and particle flow code (PFC) simulation. Notched bedding models with dimensions of 20 cm × 24 cm × 5 cm containing soft interlayer and hard interlayer were prepared. The ratio of compressive strength to tensile strength in soft gypsum and hard gypsum are 12 and 7.8, respectively. The layer angel changed from 0° to 90° with an increment of 15°. The lengths of notches in each model are similar and were equal to 20 mm, 40 mm, and 60 mm. Models were tested by Punch shear by displacement loading rates of 0.05 mm/min. Results showed that pure tensile fracture was developed from the tip of the notch, and propagated in the direction of the shear loading axis till coalescence with the model boundary. Whereas soft brittle gypsum has less deformability in comparison to hard ductile gypsum therefore the continuity of shear displacement associated with crack growth in soft interlayer was less than that in hard interlayer. Also, soft brittle gypsum has less shear strength in comparison to hard ductile gypsum therefore the shear strength of bedding rock has maximum value when hard ductile gypsum was occupied more percentage of shear surfaces. The failure mechanism was alike in both the numerical simulation and the experimental test.

## Keywords

bedding rock, soft interlayer, hard interlayer, PFC2D

## 1 Introduction

High degree of anisotropy is represented by a significant part of bedding rocks of sedimentary origin in the upper layers of the earth's crust [1–5]. As one of the most pivotal items in rock engineering, anisotropy must be investigated exactly whether it is applied in mining, civil, petroleum and geo environmental engineering. Seismic, mechanical, thermal, and hydraulic behavior of rocks which differ in various orientations may influenced by presence of hard and soft layers. If rock bedding layers' behavior is not takes into account in engineering projects, according to the expanse of rock anisotropy errors may happen in various amounts [6–7]. Based on the spacing of bedding planes, sedimentary rocks can be considered as isotropic or anisotropic [8]. Especially when non-persistent or persistent joints were developed thought these rocks (Fig. 1).

Concurrent with bedding layer weak plane, non-persistent joint is defined as one kinds of discontinuity which declines the rock strength and lead to rock instability [9–15].

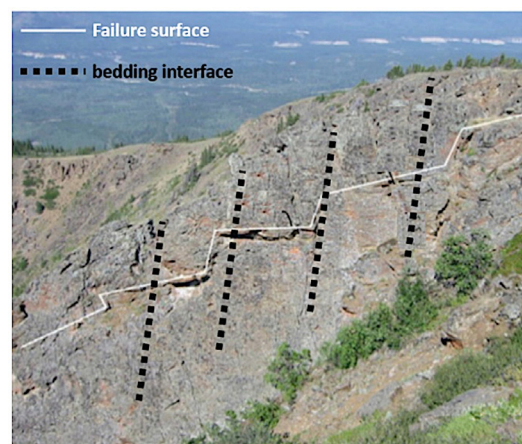


Fig. 1 Bedding layer with non-persistent joints [2]

Therefore, the significance of evaluating the failure behavior of notched rock under test is proved by instabilities of layered rock containing discontinuities [16]. Preceding research widely concentrated on the mechanical and failure

mechanism of one-layer rock mass containing joint utilizing the physical [17–21] and numerical techniques [22–23]. Four kinds of cracks including coplanar frictional crack, oblique frictional crack, tensile cracks, and anti-wing cracks and seven modes of joints coalescence including shear crack, splitting crack, mixed mode crack, etc. were reported by Zhao et al. [24] and Wang et al. [13]. Four sorts of stress strain diagrams of non-persistent jointed rock were specified according to the coalescence of pre-existed joints and number of cracks at the post-peak phase [25]. Prudencio and Van Sint Jan [20] during the assessment of mechanical properties of notched rock found out that strength parameter remarkably depends on failure mode; while the strength related to the rotational breakage is relatively low, the strength of rock mass sliding failure is high. By conducting UCS test on the rock like notched material with various notch angles, Kulatilake et al. [26] found three failure modes for the jointed rock model proposed by aforementioned researchers. The experiment outcomes show that the failure mechanism of notched rock is changed with the notch angel. Tien et al. [27] have been studied the failure mechanism of anisotropic rock under different loading condition. They utilized a rock like material consist of an admixture of kaolinite and cement. Failure patterns were included of sliding failure along discontinuities, sliding failure a cross discontinuity, pure tensile crack, and split-tensile along weak plane. Many resemblances in terms of the fracture patterns and process can be observed between the Kulatilake et al. [26] test results and Tien et al. [27] outputs. Whereas the continuous formation of parallel layers forms the soft-hard interbedded rocks therefore the loading capacity of bedding rock is imperceptible compared to the strength of the rock mass. Extensive studies have focused on the failure characteristics of bedding rock, lead to more attention to this research field. Nonetheless, this consideration has been concentrated on the study of failure mechanism of bedding rock under physical UCS test [27–29], theoretical methods [30] or by numerical modelling [31]. Zhao et al. [32] studied the effect of boundary conditions on the failure mechanism of bedding rock. In some research, the influence of angel of layer angles on the failure mechanism of bedding rock has been analyzed [33]. Many researchers employed materials like gypsum and cement to provide layered rock-like materials in laboratory tests to control the inclination and position of bedding planes, effectively [34–37]. Whereas the majority of collapse failures were occurred in anisotropic rock mass therefore the investigation of shear behavior of notched

bedding rock is very useful for safety design of rock mass engineering structures. This study presents the influence of angel of layer and brittleness of layer on the failure behavior of notched bedding rock utilizing experimental punch shear test and PFC simulation. In this way, the PFC was calibrated firstly by both UCS test and Brazilian test. Secondly, verification of numerical outputs has been done with results of experimental shear test. Finally, the comprehensive study was performed on the shear behavior of notched bedding models.

## 2 Physical test

### 2.1 Make the hard gypsum and soft gypsum specimens

To make hard ductile plaster specimens, the amount of water/Polyvinyl acetate/gypsum was chosen as 2/0.043/1.3. First, gypsum was dissolved in water. Then polymer material was added, and plaster slurry was cast into the mold. For making soft brittle plaster specimens, the ratio of water to gypsum was determined equal to 2/1. Cylindrical specimens had a height of 108 mm and a diameter of 54 mm, and the disk specimens had a height of 27 mm, and a diameter of 54 mm. Samples were tested under Uniaxial compression test (UCS) and Brazilian test. Five similar samples were prepared for each test. Fig. 2(a) and b represent the failure pattern of soft and hard gypsum under UCS test and Brazilian test. Uniaxial compressive strength, tensile strength and Young Modulus of hard gypsum are 12.2 MPa, 1.55 MPa and 8.4 GPa, respectively. Uniaxial compressive strength, tensile strength and Young Modulus of soft gypsum are 7.8 MPa, 0.65 MPa and 3.95 GPa, respectively.

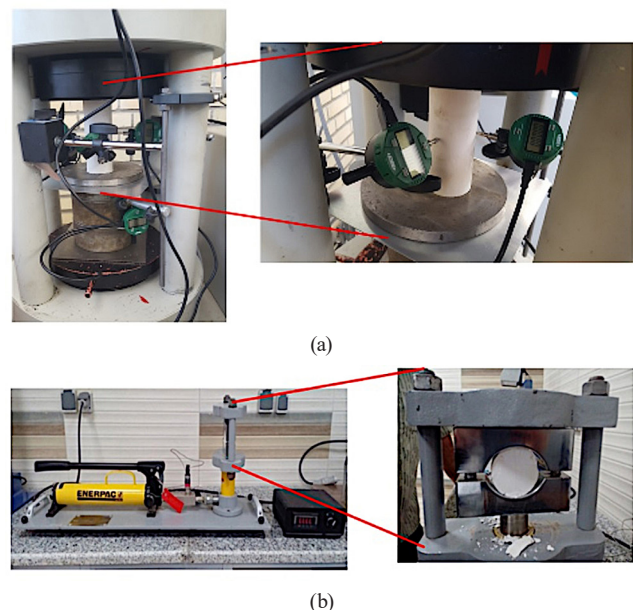


Fig. 2 (a) UCS test and (b) Brazilian test

The ratio of compressive strength to tensile strength in soft gypsum and hard gypsum are 12 and 7.8, respectively. It shows that brittle failure was occurred in soft gypsum while ductile failure was happened in hard gypsum.

**2.2 Preparing the notched bi-material layers**

A box with dimensions of 200 mm × 240 mm × 50 mm was utilized to build the main cast (Fig. 3(a)). The oily sheet (Plexiglas) is placed in the upper and lower notches. The slurry enters into the mold via the upper opening. To prepare three layered samples, at first, hard gypsum slurry was poured into the mold. Following 25 minutes, the soft gypsum slurry was poured into the mold and finally hard gypsum slurry was poured into the mold. After 25 minutes, the mold was opened, and the sample was removed from the mold. The Plexiglas sheets were removed from the sample so two notches were prepared in the specimen (Fig. 3(b)). Thickness of soft gypsum in hard interlayered model and soft interlayered model was 160 mm (Fig. 3(c)) and 80 mm (Fig. 3(d)), respectively. Each model was consisted of two parallel edge notches (a in Fig. 3(c)) with lengths of 20 mm, 40 mm and 60 mm. Opening of the notches were 1 mm. Table 1 show the samples containing

three layers with various edge notch length. After locating the samples in a 22°C condition for 30 days, the notched bedding rock tested in punch shear test condition using a servo control compression test device. The UCS device includes the test bed, loading control system, and data acquisition system. The sample was located in the base and maintained the horizontal contacts with the base. Special geometry of specimen induces direct shear load on the samples (Fig. 3(e)). Over the experiments, the displacement loading rates were controlled to 0.05 mm/min. For calculation of shear stress, the applied force was divided to shear surface that is equal to 24 cm × 5 cm.

**2.3 Experimental observations**

**2.3.1 Failure pattern of layered samples**

In three layers notched sample with hard gypsum interlayer (Table 2(a)–(c)), one tensile crack was initiated from notch tip situated in lower soft layer and turned left for a small distance. This crack was propagated parallel to shear loading direction and go via the two interfaces till reach to the upper notch tip. In the three-layer notched models with soft gypsum interlayer (Table 2(d)–(f)), a single tensile crack originated from the lower notch tip located

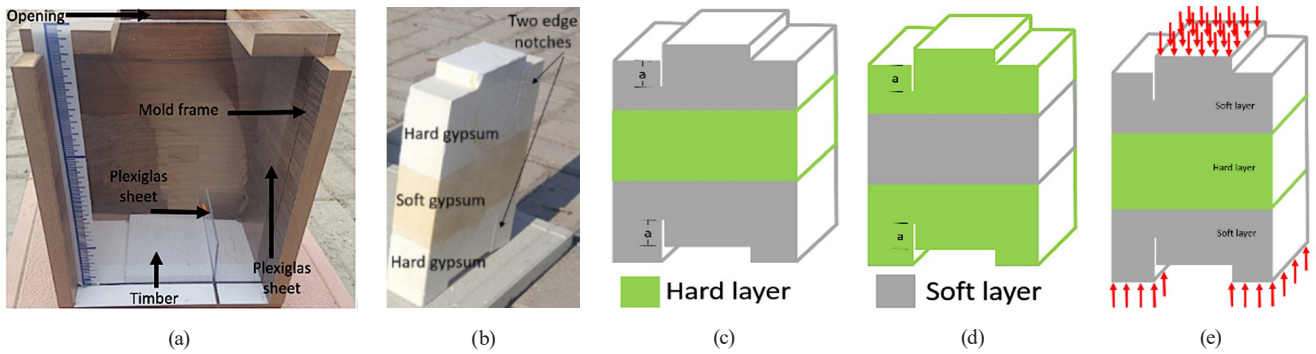


**Fig. 3** (a) MDF mold, (b) physical notched layered specimen, (c) three layered model with hard interlayer, (d) three layered model with soft interlayer and (e) notched bedding layer under punch shear test

**Table 1** Three layered samples containing hard interlayer and soft interlayer with different notch length

| Soft layer number/hard layer number = 2/1 |     |     | Soft layer number/hard layer number = 1/2 |     |     |
|---|-----|-----|---|-----|-----|
| Notch length (each notch in cm)           |     |     | Notch length (each notch in cm)           |     |     |
| 2   | 6   | 6   | 2   | 6   | 6   |
|   |     |     |   |     |     |
| (a)                                       | (b) | (c) | (d)                                       | (e) | (f) |

in the hard gypsum layer, turned left for a short distance, and was propagated parallel to the shear loading direction until it reached the lower interface of layers. Subsequently, this tensile crack progressed through the soft gypsum layer until it reached the second layer interface and continued through the upper hard gypsum layer until it reached the upper boundary of the sample. In the study, it was observed that when the length of the notch was 4 cm, there was a noticeable change in the direction of the tensile crack initiation in newborn samples. Specifically, the crack turned towards the right and propagated upwards towards the boundary of the sample. Differences between this failure pattern (Table 2(e)) and failure patterns of both 2 cm and 6 cm notched sample (Table 2(d) and (f)) is due to differences in position of pre-existing notches in the samples.

**2.3.2 The influence of pre-existing joint length on the shear stress-shear displacement curve**

Fig. 4(a) and (b) show the shear stress-shear displacement diagram for both three-layered model with hard interlayer and three-layered model with soft interlayer, respectively.

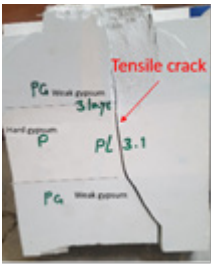
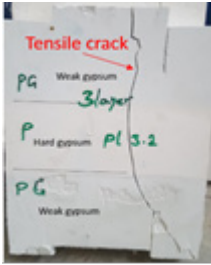
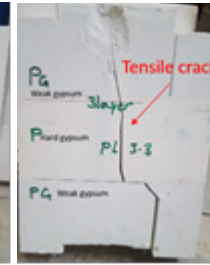
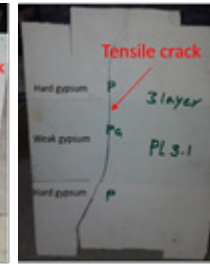
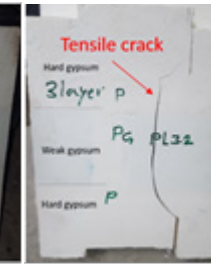
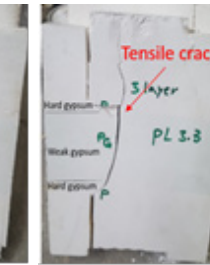
The results of the 2 cm notched model, 4 cm notched model and 6 cm notched model were presented in each figure. Dip angle of shear stress-shear displacement diagram or shear stiffness of model was reduced by enhancing the notch length. Also, the shear displacement associated to highest shear stress was reduced by enhancing the notch length. In fact, according to fracture mechanic theory, both stress intensity at the notch tips and stress interaction between the notch tips were enhanced by enhancing the notch length. These lead to reduce the shear stiffness and shear displacement associated to maximum shear stress.

**3 Numerical method**

**3.1 Discrete element method**

Discrete element technique creates particular materials by merging produced individual particles in the form of bond. Particle flow code, PFC presumes whole of generated bodies as rigid particles. Discs link each other via moment of force and internal force. Therefore, the contact can be described as point contact. The force-normal displacement and force-shear displacement laws govern the relative displacement

**Table 2** Failure patterns of three layered samples

| Soft layer number/hard layer number = 2/1   |   |   | Soft layer number/hard layer number = 1/2   |  |   |
|---|---|---|---|--|---|
| Notch length (each notch in cm)   |   |   | Notch length (each notch in cm)   |  |   |
| 2   | 6   | 6   | 2   | 6  | 6   |
|  |  |  |  |  |  |
| (a)   | (b)   | (c)   | (d)   | (e)  | (f)   |

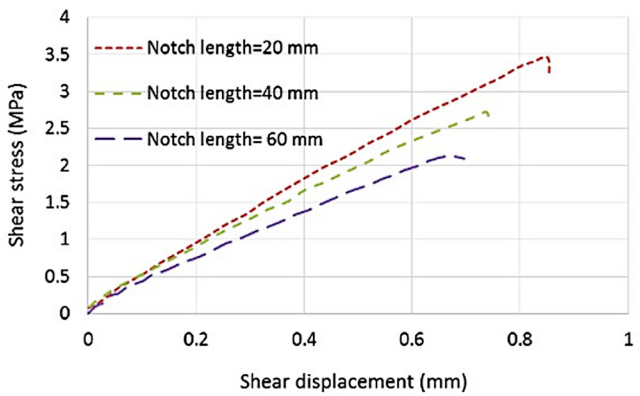
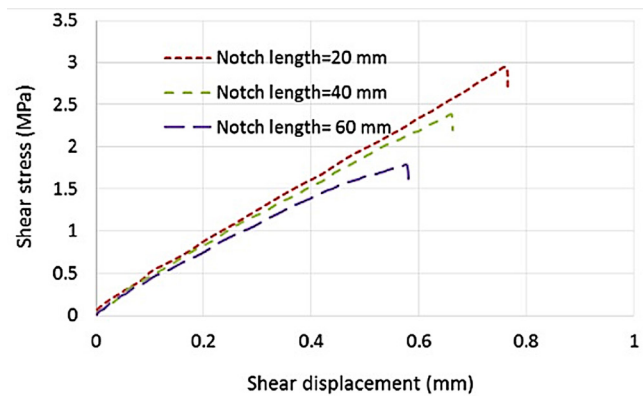


**Fig. 4** shear stress-shear displacement curve for three layered model with (a) hard interlayer and (b) soft interlayer

between discs, which correlated with the contact stress [38]. There is a connection bond at the contact, and the interaction can be calculated by employing the potential energy function. Whereas Particle flow code enables large deformation and fracture and separation of the macro structure and deformation, or fracture is applied by transmission and rotation of the discs. A considerable part of the deformation in a physical system is defined as motion along the interface. Deformation is mostly due to the interaction between the particles that operate on rigid objects rather than the deformation of individual particles. In the theory of discrete elements, as soon as the internal force attains equilibrium, the interaction between discs can be considered as a dynamic process in equilibrium state. The applied force to the discs and of the particle displacement can be measured by monitoring the movement of each disc. The dynamic step length can be characterized in time steps by presuming the speed and accelerated speed are fixed for each time step. By selecting explicit numerical computational technique to simulate nonlinear interactions between great number of discs, extreme storage and iterations are obstructed [39]. Since discs paste to each other via flat-joint (FJ) model in this paper, the object formed by discs can be considered as brittle materials. The interface of FJ model consists of units, and the fracture of FJ units will lead to local fracture of the interface, and the failure of interfacial contacts leads to cracks. The contact interface of particles in a FJ model is sectioned. As soon as the contact touches yield conditions, the bonding effect is vanished. The bonding state is elastic and linear. The units can be un-bonded or bonded and the cracks will not merge or overlap each other. By flat joint model it is possible to calibrate both tensile strength and compressive strength correctly and simultaneously [39].

### 3.2 Calibration of micro-parameters of FJ model and Smooth joint model

In particle flow code, the setting of material characteristics is managed via describing inter-granular micro-parameters,

i.e., electing inter-granular characteristics that ensure whole of the macroscopic mechanical characteristics of rock are delivered. Via UCS and typical Brazilian tests, the parameters usually will be calibrated. The model can be employed to simulate the material as soon as a specified set of inter-granular micro-parameters is consistent with all the macro-mechanical characteristics of the material. In order to debugging, the identical modulus of elasticity as the macroscopic one is chosen. The failure mode of the sample is controlled by regulating the normal to tangential bond strength ratio. Through uniaxial compression test and Brazilian test, elasticity modulus, compressive strength  $\sigma_c$  and tensile strength  $\sigma_t$  were calibrated for both of the soft gypsum and hard gypsum. FJ Micro properties for both soft and hard gypsum models used in this study are tabulated in Table 3.

Porosity of model was chosen as 0.08 according to PFC manual to obtain the best compaction of model material. Damping factor was 0.7 to stablish the static condition. Macro Young modulus of model was affected by both Young modulus of flat joint and Young modulus of disc contacts. Poisson ratio of model was affected by both stiffness of flat joint and stiffness of disc contacts. Compression strength and tensile strength of model were calibrated by cohesion of flat joint model and tensile strength of flat joint model, respectively. Crack initiation stress was calibrated by standard deviation flat joint cohesion and standard deviation flat joint tensile strength. As for the calibrated model, Young's modulus of soft gypsum  $E = 4$  GPa, compressive strength of soft gypsum  $\sigma_c = 7.9$  MPa, and tensile strength of soft gypsum  $\sigma_t = 0.7$  MPa. Also, Young's modulus of hard gypsum  $E = 8.3$  GPa, compressive strength of hard gypsum  $\sigma_c = 12.35$  MPa, and tensile strength of hard gypsum  $\sigma_t = 1.61$  MPa. The interval can be recognized between reference amounts and calibrated outcomes is relatively minor, means the micro-parameters can be employed to describe soft gypsum and hard gypsum.

**Table 3** Micro parameters of both of the soft gypsum and hard gypsum

| Particle micro properties                  | Soft model | Hard model | FJ Micro properties                          | Soft model | Hard model |
|--|------------|------------|--|------------|------------|
| Minimum particle radius (mm)               | 0.15       | 0.13       | Young modulus (GPa)                          | 5          | 8          |
| Particle radius ratio                      | 1.6        | 1.5        | Friction (°)                                 | 32         | 39         |
| Normal stiffness to shear stiffness ration | 1.3        | 1.5        | FJ bond tensile strength (MPa)               | 0.5        | 1.4        |
| Density (kg/m <sup>3</sup> )               | 2400       | 2600       | Standard deviation of tensile strength (MPa) | 0.05       | 0.14       |
| Young modulus (GPa)                        | 5          | 8          | FJ bond cohesion (MPa)                       | 5          | 10         |
|  |            |            | Cohesion standard deviation (MPa)            | 0.5        | 1          |
|  |            |            | Normal stiffness to shear stiffness ration   | 1.3        | 1.5        |

The smooth joint model (SJM) simulates the behavior of a smooth interface, irrespective of the local particle contact directions along the interface [40]. The interface between soft gypsum and hard gypsum was created by the SJM in this paper. Smooth joint model will be used when a weak plane exists in the model. SJM only was adjusted in the interfaces between hard gypsum and soft gypsum. Whereas there are not any weak planes in the hard rock and soft rock therefore SJM is not applicable for other situations. Both of the experimental indirect tensile test and numerical indirect tensile test were done on the bi-material disc to specify the micro parameters of SJM (Normal stiffness = 350 GPa/m, Shear stiffness = 200 GPa/m, Friction coefficient = 0.8 and Large strain flag = 1). Fig. 5 shows the schematic of Brazilian test on bi-material disc.

The tensile strength of contact surface between soft gypsum and hard gypsum were 1.83 MPa and 1.86 MPa in laboratory test and numerical simulation, respectively. This demonstrates that the numerical result achieves a good agreement with laboratory tests. Whereas the tensile strength of contact interface (1.86 MPa) is more than

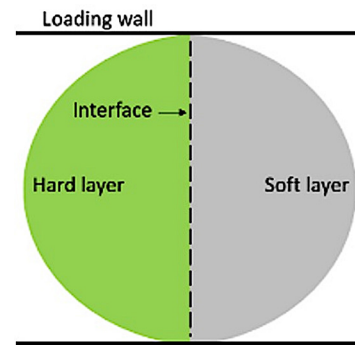


Fig. 5 Schematic view of Brazilian test on bi-material disc

both tensile strength of soft gypsum (0.65 MPa) and tensile strength of hard gypsum (1.55 MPa) therefore it can be concluded that welded interface, with high tensile strength, exists between the soft gypsum and hard gypsum.

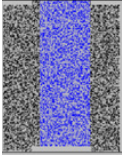
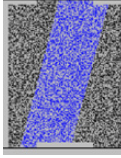
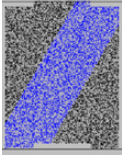
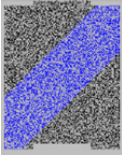
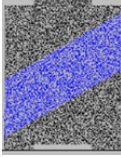
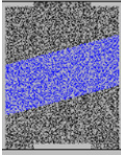
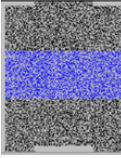
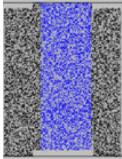
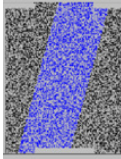
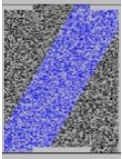
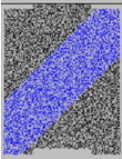
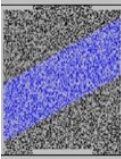
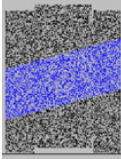
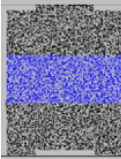
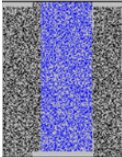
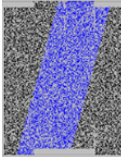
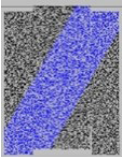
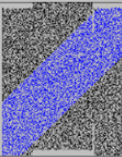
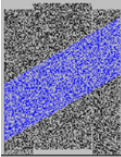
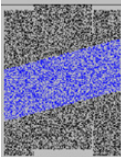
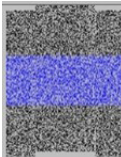
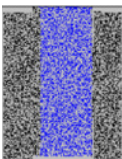
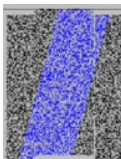
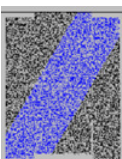
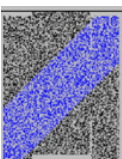
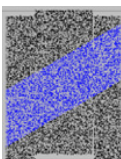
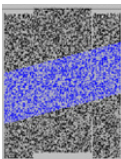
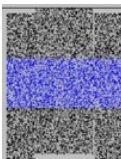
### 3.3 Model development by PFC

A model with dimension of 240 mm × 200 mm in PFC<sup>2D</sup> which includes three layers with soft interlayer and hard interlayer were simulated to be tested under punch shear tests (Table 4 and Table 5).

Table 4 Bedding models; gray and blue colors are representative of hard and soft gypsum, respectively

| Bedding layer angle (°) |     |     |     |     |      |      |
|-------------------------|-----|-----|-----|-----|------|------|
| 0                       | 15  | 30  | 40  | 60  | 75   | 90   |
|                         |     |     |     |     |      |      |
| (a)                     | (b) | (c) | (d) | (e) | (f)  | (g)  |
|                         |     |     |     |     |      |      |
| (h)                     | (i) | (j) | (k) | (l) | (m)  | (n)  |
|                         |     |     |     |     |      |      |
| (o)                     | (p) | (q) | (r) | (s) | (t)  | (u)  |
|                         |     |     |     |     |      |      |
| (v)                     | (w) | (x) | (y) | (z) | (aa) | (bb) |

**Table 5** Bedding models; gray and blue colors are representative of hard and soft gypsum, respectively

| Bedding layer angle (°)   |   |   |   |  |   |   |
|---|---|---|---|--|---|---|
| 0   | 15  | 30  | 40  | 60   | 75  | 90  |
|    |    |    |    |    |    |    |
| (a)   | (b)   | (c)   | (d)   | (e)  | (f)   | (g)   |
|    |    |    |    |    |    |    |
| (h)   | (i)   | (j)   | (k)   | (l)  | (m)   | (n)   |
|    |    |    |    |    |    |    |
| (o)   | (p)   | (q)   | (r)   | (s)  | (t)   | (u)   |
|  |  |  |  |  |  |  |
| (v)   | (w)   | (x)   | (y)   | (z)  | (aa)  | (bb)  |

Each model consisted of two parallel edge notches with lengths of 20, 40, and 60 mm and an opening of 1 mm (Table 4 and Table 5). Bedding layer angles altered from 0° to 90° with increment of 15°. Each model was consisted of two parallel edge notches with lengths of 20 mm, 40 mm and 60 mm. Opening of the notches were 1 mm. Thickness of soft gypsum in horizontal hard interlayered model and horizontal soft interlayered model was 160 mm (Table 4(g)) and 80 mm (Table 5(g)), respectively. Two horizontal bands of particles with wide of 10 mm were removed from top of the model in both of left side and right side. Also, one horizontal band of particles was removed from bottom of model in the middle to create the punch shear test condition. The upper and lower walls were moved near one another at a velocity of 0.016 m/s to simulate the punch shear test. The shear displacement was calculated using the displacements of the upper wall. In order to evaluate the applied shear force, put forth on the modeled sample, the reaction forces on the upper wall were documented. For the calculation of applied shear

stress, 50% of applied force was divided into the one shear surface that is equal to 240 mm due to double shear condition. Totally 56 models were subjected to punch shear test.

#### 4 Numerical results

##### 4.1 Failure patterns of numerical models

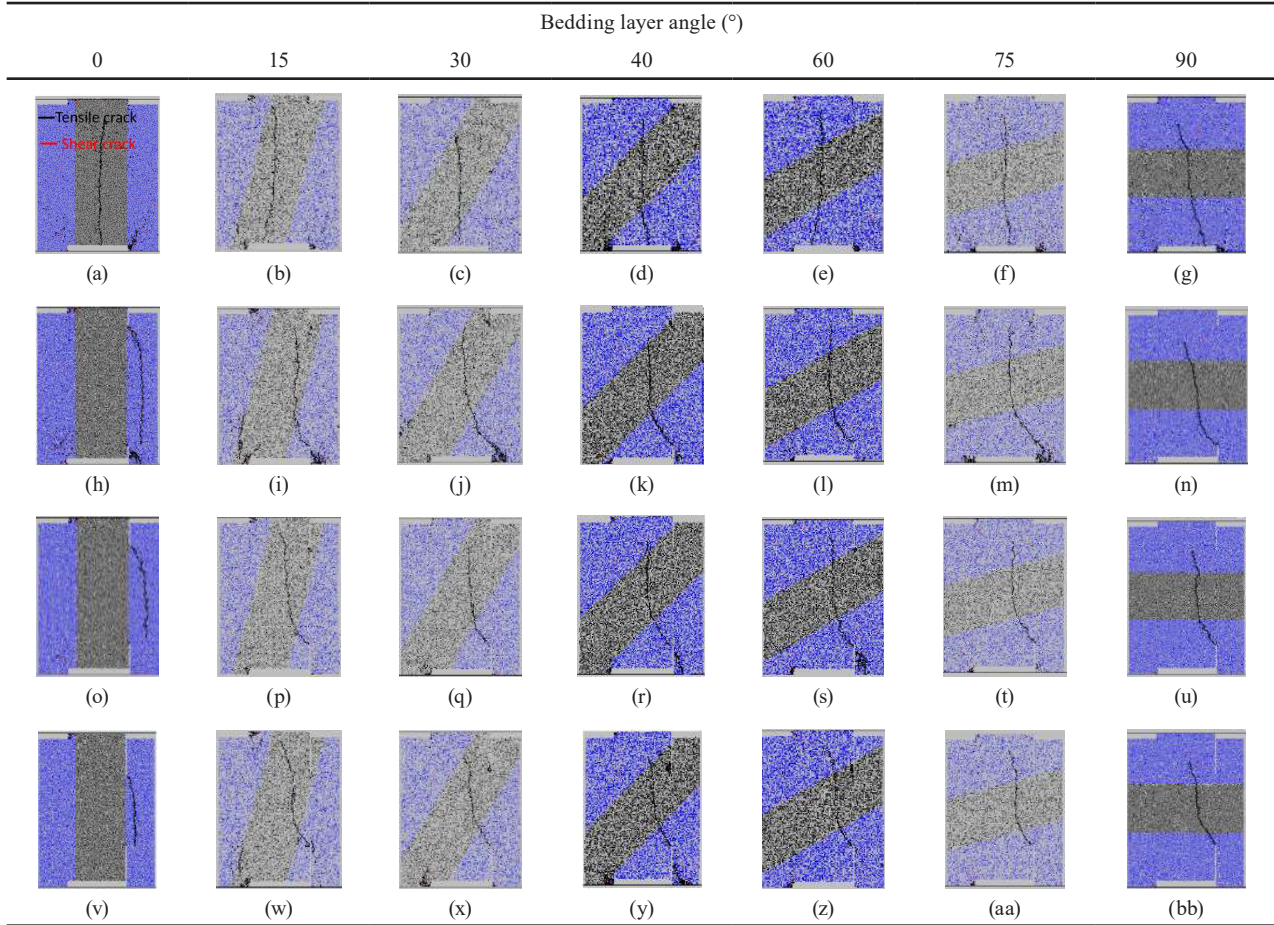
##### 4.1.1 Failure pattern of three-layered model with hard interlayer

Table 6 displays the failure patterns of three-layer models with hard interlayers, with variations bedding angles and edge notch lengths. Gray color and blue color are hard gypsum and soft gypsum, respectively. Also, black line and red line represent the tensile crack and shear crack, respectively.

##### a) Intact model

When the bedding layer angles were 0° and 15° (Table 6(a) and (b)), a single tensile crack started from the middle of the lower boundary in hard gypsum layer. This crack propagated upwards in the vertical axis until it reached the upper boundary of the hard gypsum. When bedding layer

**Table 6** Failure patterns of three-layered model with hard interlayer; gray and blue colors are representative of hard and soft gypsum, respectively



angle were more than 15° (Table 6(c)–(g)), a single tensile crack started from the middle of the lower boundary in soft gypsum layer. This crack propagated upwards in the vertical axis until it reached the lower interface of the soft gypsum and hard gypsum layers. After passing through the hard interlayer, the crack reached the upper interface of the hard gypsum and soft gypsum layers and continued to propagate through the second soft gypsum layer until it reached the upper boundary of the soft gypsum.

**b) Notch length = 2 cm**

When bedding layer angle was 0° (Table 6(h)), a single tensile crack initiated at the upper notch tip in the soft gypsum layer and turned right for a short distance. It is followed by a parallel propagation to the direction of shear loading until it reaches the lower notch tip. The propagation of a crack was observed across the soft gypsum material along its entire trajectory.

When bedding layer angles were more than 0° (Table 6(i)–(n)), a single tensile crack initiated at the lower notch tip in the soft gypsum layer and turned left for a short distance. This crack propagated upwards in the

vertical axis until it reached the lower interface of the soft gypsum and hard gypsum layers. After passing through the hard interlayer, the crack reached the upper interface of the hard gypsum and soft gypsum layers and continued to propagate through the second soft gypsum layer until it reached the upper boundary of the soft gypsum.

**c) Notch length = 4 cm and 6 cm**

When bedding layer angle was 0° (Table 6(o) and (v)), a single tensile crack initiated at the upper notch tip in the soft gypsum layer and turned right for a short distance. It is followed by a parallel propagation to the direction of shear loading until it reaches the lower notch tip. The propagation of a crack was observed across the soft gypsum material along its entire trajectory.

When bedding layer angles were more than 0° (Table 6(p)–(u) and Table 6(w)–(bb)), a single tensile crack started at the lower notch tip in the soft gypsum layer and turned left for a short distance. This crack propagated upwards in the vertical axis until it reached the lower interface of the soft gypsum and hard gypsum layers. After passing through the hard interlayer, the

crack reached the upper interface of the hard gypsum and soft gypsum layers and continued to propagate through the second soft gypsum layer until it reached the upper boundary of the soft gypsum. It's to be note that, in constant notch length, the crack growth length in soft layer increased by increasing the layer angle while its length in hard layer was decreased. In constant layer angle, the crack growth length in soft layer decreased by increasing the notch length while its propagation length in hard layer is constant. By comparison between Table 2(a), (b) and (c) and Table 6(n), (u) and (bb), it can be concluded that the failure patterns of hard interlayered models with layer angle of 90° are similar to those of physical samples.

#### 4.1.2 Failure pattern of three-layered model with soft interlayer

Table 7 displays the failure patterns of three-layer models with soft interlayers, with variations bedding angles and edge notch lengths. Gray color and blue color are hard gypsum and soft gypsum, respectively. Also, black line and red line represent the tensile crack and shear crack, respectively.

##### a) Intact model

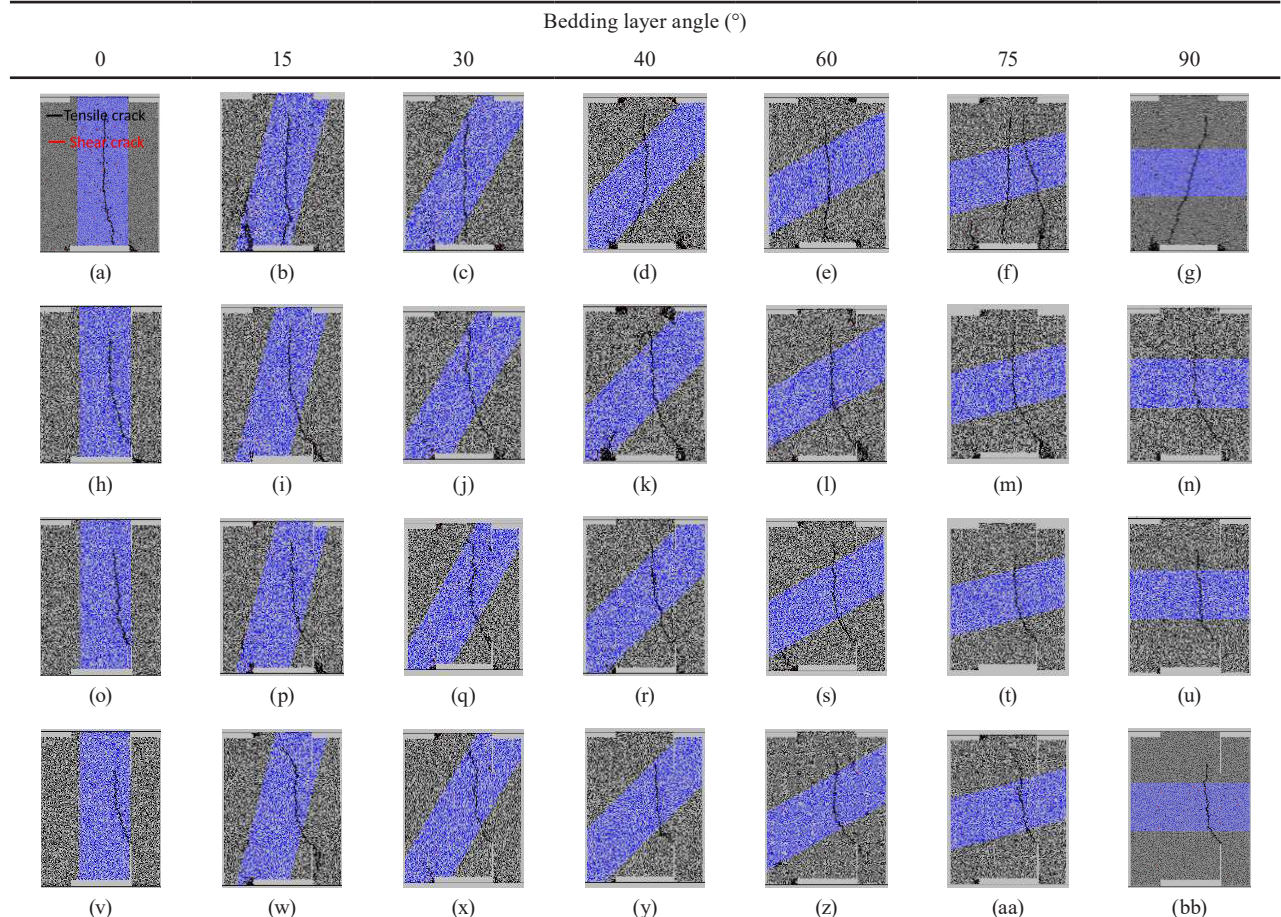
When bedding layer angle were 0° and 15° (Table 7(a) and (b)), a single tensile crack started from the middle of the lower boundary in soft gypsum layer. This crack propagated upwards in the vertical axis until it reached the upper boundary of the soft gypsum.

When bedding layer angle were more than 15° (Table 7(c)–(g)), a single tensile crack started from the middle of the lower boundary in hard gypsum layer. This crack propagated upwards in the vertical axis until it reached the lower interface of the hard gypsum and soft gypsum layers. After passing through the soft interlayer, the crack reached the upper interface of the soft gypsum and hard gypsum layers and continued to propagate through the second hard gypsum layer until it reached the upper boundary of the hard gypsum.

##### b) Notch length = 2 cm

When bedding layer angle was 0° (In Table 7(h)), a single tensile crack started at the lower notch tip in the soft gypsum layer and turned left for a short distance. It is followed by a parallel propagation to the direction of shear loading

**Table 7** Failure patterns of three-layered model with soft interlayer; gray and blue colors are representative of hard and soft gypsum, respectively



until it reaches the upper notch tip. The propagation of a crack was observed across the soft gypsum material along its entire trajectory. When bedding layer angles were more than  $0^\circ$  (In Table 7(i)–(n)), a single tensile crack started at the lower notch tip in the hard gypsum layer and turned left for a short distance. This crack propagated upwards in the vertical axis until it reached the lower interface of the hard gypsum and soft gypsum layers. After passing through the soft interlayer, the crack reached the upper interface of the soft gypsum and hard gypsum layers and continued to propagate through the second hard gypsum layer until it reached the upper boundary of the hard gypsum.

c) Notch length = 4 cm and 6 cm

When bedding layer angle was  $0^\circ$  (Table 7(o) and (v)), a single tensile crack started at the lower notch tip in the soft gypsum layer and turned left for a short distance. It is followed by a parallel propagation to the direction of shear loading until it reaches the upper notch tip. The propagation of a crack was observed across the soft gypsum material along its entire trajectory.

When bedding layer angles were more than  $0^\circ$  (Table 7(p)–(u) and Table 7(w)–(bb)), a single tensile crack started at the lower notch tip in the hard gypsum layer and turned left for a short distance. This crack propagated upwards in the vertical axis until it reached the lower interface of the hard gypsum and soft gypsum layers. After passing through the soft interlayer, the crack reached the upper interface of the soft gypsum and hard gypsum layers and continued to propagate through the second hard gypsum layer until it reached the upper boundary of the hard gypsum. It is to be note that, in constant notch length, the crack growth length in hard layer increased by increasing the layer angle while its length in soft layer was decreased.

In constant layer angle, the crack growth length in hard layer decreased by increasing the notch length while its propagation length in soft layer is constant. By comparison between Table 2(a), (b) and (c) and Table 7(n), (u) and (bb), it can be concluded that the failure patterns of soft interlayered models with layer angle of  $90^\circ$  are similar to those of physical samples.

#### 4.2 Rose diagram of crack growth

Table 8 represents Rose diagram of crack growth in hard interlayered model and soft interlayered model with bedding angle of 75 degrees, respectively. The results of 2 cm notched model, 4 cm notched model and 6 cm notched model were presented in Table 8.

In all configurations, the angles between micro cracks and horizontal axis changed from 75 to 105 degrees, which shows that the variations of notch length and bedding layer mechanical properties have not important influence on angle of the major fractures. Also in constant notch length, for example notch length of 2 cm, the cracks numbers in soft interlayered model (Table 8(a)) was more than that in hard interlayered model (Table 8(d)). Because crack growth length in soft interlayer (Table 7(m), (t), (aa)) was more than that in hard interlayered model in this layer angle (Table 6(m), (t), (aa)). Whereas the soft interlayer has brittle behavior in comparison to hard ductile interlayer therefore cracks numbers in soft interlayered model was more than that in hard interlayered model.

#### 4.3 Influence of model brittleness on the shear stiffness

Fig. 6(a)–(c) represents the influence of layer angle on the shear stiffness of bedding model. This figure for notch length of 2 cm, 4 cm and 6 cm were divided to three sections.

**Table 8** Rose diagram of cracks in models with bedding angle of  $75^\circ$  containing different notch lengths

| (Hard layer / soft layer) | Notch length (one notch in cm) |   |   |
|---------------------------|--------------------------------|---|---|
|                           | 2                              | 4 | 6 |
| (2/1)                     |                                |   |   |
| (1/2)                     |                                |   |   |

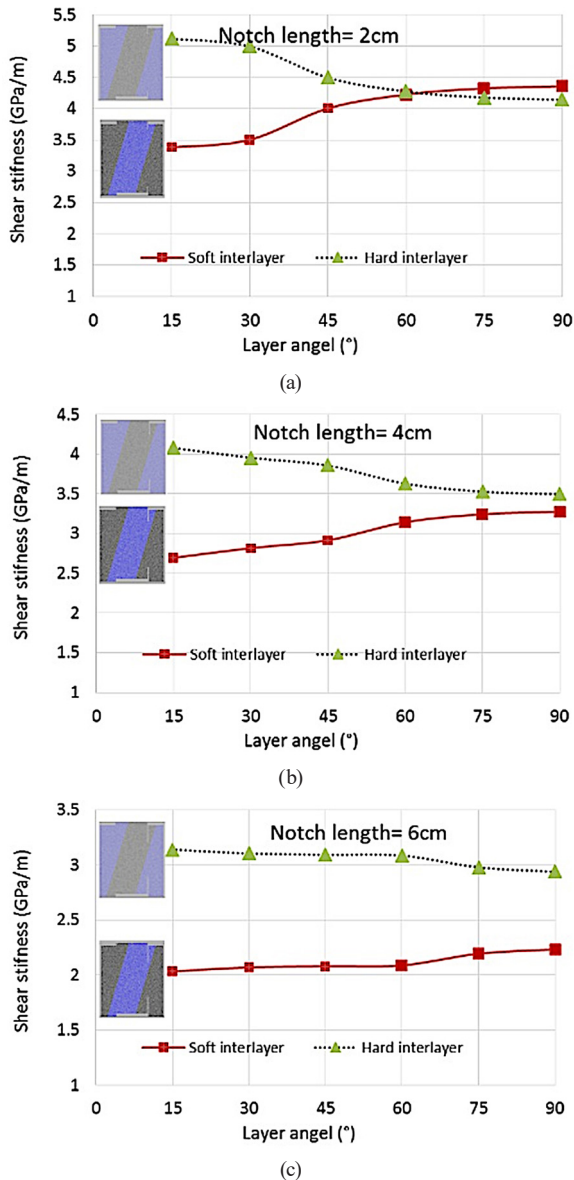


Fig. 6 Effect of layer angle on shear stiffness for notch length of, (a) 2 cm, (b) 4 cm and (c) 6 cm

Totally, the shear stiffness of hard interlayered model was decreased by increasing the layer angle while shear stiffness of soft interlayered model was increased by increasing the layer angle. In hard interlayered model, the crack growth length in hard ductile layer was decreased by increasing the layer angle (Table 6) while crack growth length in soft interlayered was increased by layer angle (Table 7). Whereas the mechanical properties of hard ductile gypsum are more than that of soft brittle gypsum Therefore shear stiffness of hard interlayered model was reduced by enhancing the layer angle. When notch length was 2 cm and layer angle was less than 60°, shear stiffness of hard interlayered model was more than that of soft interlayered model. When layer angle was more than 60°,

shear stiffness of soft interlayered model was more than that of hard interlayered model. In other word, when layer angle was less than 60°, crack growth length in hard ductile layer was more than that in soft interlayered model while crack growth length in hard ductile layer was less than that in soft interlayered model for layer angle of more than 60°. Whereas the mechanical properties of hard ductile gypsum are more than that of soft brittle gypsum, therefore shear stiffness of hard interlayered model was more than that of soft interlayered model for layer angle of less than 60°. When notch lengths were 4 cm and 6 cm, shear stiffness of hard interlayered model was more than that of soft interlayered model for any layer angle. In these configurations, crack growth length in hard ductile layer was more than that in soft interlayered model. Whereas the mechanical properties of hard ductile gypsum are more than that of soft brittle gypsum, therefore shear stiffness of hard interlayered model was more than that of soft interlayered model for any layer angle.

#### 4.4 Influence of notch length on the shear stiffness

Fig. 7(a)–(g) represents the effect of notch length on the shear stiffness. This figure for different layer angles was divided to seven sections.

The results of hard interlayered model and soft interlayered model were presented in each figure. When layer angle was 0° (Fig. 7(a)), shear stiffness's were similar in hard interlayered model and soft interlayered mode. Whereas tensile cracks were developed completely through soft brittle gypsum in these configurations (Table 6(h), (o), (v) and Table 7(h), (o), (v)), therefore their shear stiffness's are nearly similar, too. When layer angles were 15°, 30° and 45° (Fig. 7(b)–(d)), totally shear stiffness was reduced by enhancing the notch length. This behavior can be attributed to fracture mechanics theory, wherein the stress intensity at the notch tips and the stress interaction between the notch tips is amplified by increasing the notch length, leading to lower shear stiffness. Shear stiffness of hard interlayered model was more than that of soft interlayered model for any notch length. In these configurations, crack growth length in hard ductile layer (Table 6(i)–(k), (p)–(r), (w)–(y)) was more than that in soft interlayered model (Table 7(i)–(k), (p)–(r), (w)–(y)). Whereas the shear stiffness of hard ductile gypsum is more than that of soft brittle gypsum, Therefore, shear stiffness of hard interlayered model was more than that of soft interlayered model for layer angle of 15°, 30° and 45°. By increasing the layer angle from 15° to 45°, differences between the shear

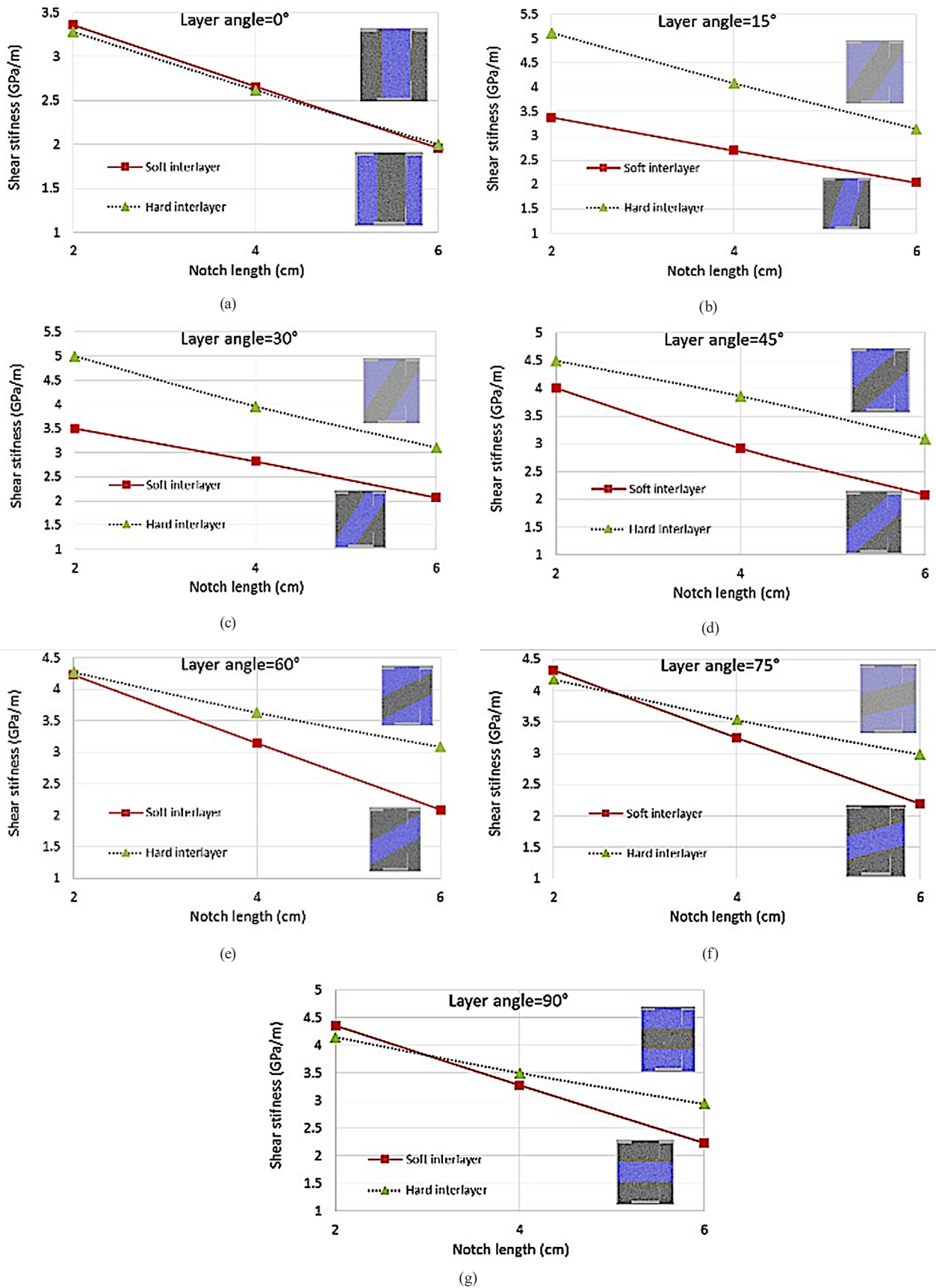


Fig. 7 Effect of notch length on shear stiffness of models with layer angle of, (a) 0°, (b) 15°, (c) 30°, (d) 45°, (e) 60°, (f) 75 and (g) 90°

stiffness of hard interlayered model and soft interlayered model was decreased due to increasing the presence of soft brittle gypsum in shear surface direction (Fig. 5(b)–(d)). When layer angles were 60°, 75° and 90° (Fig. 5(e)–(g)), totally shear stiffness was reduced by enhancing the notch length. When notch length was 2 cm, shear stiffness of 60° hard interlayered model was less than that of soft interlayered model. Because in this configuration, crack growth length in hard ductile layer (Table 6(l)–(n)) was less than that in soft layer (Table 7(l)–(n)). When notch lengths were 4 cm and 6 cm, shear stiffness of hard interlayered model was more than those of soft interlayered model. In these configurations, crack growth length in hard ductile layer (Table 6(s)–(u), (z)–(bb)) was more than that in soft interlayered model (Table 7(s)–(u), (z)–(bb)). By increasing the layer angle from 60° to 90°, differences between the shear stiffness of hard interlayered model and soft interlayered model was decreased due to increasing the mobilization of soft brittle gypsum in shear surface direction in hard interlayered model (Table 6(l)–(n), (s)–(u), (z)–(bb)).

**4.5 Influence of model brittleness on the shear strength**

Fig. 8(a)–(c) represents the influence of layer angle on the shear strength. This figure for notch length of 2 cm, 4 cm and 6 cm were divided to three sections. Totally, the shear strength of hard interlayered model was decreased by increasing the layer angle while shear strength of soft interlayered model was increased by increasing the layer angle. In hard interlayered model, the crack growth length in hard ductile layer was decreased by increasing the layer angle (Table 6) while in soft interlayered model, crack growth length in hard layer was increased by increasing layer angle (Table 7). Whereas the mechanical properties of hard ductile gypsum is more than that of soft brittle gypsum, therefore shear strength of hard interlayered model was reduced by enhancing the layer angle. When notch length was 2 cm and layer angle was less than 60°, shear strength of hard interlayered model was more than that of soft interlayered model. When layer angle was more than 60°, shear stiffness of soft interlayered model was more than that of hard interlayered model. In other word, when layer angle was less than 60°, crack growth length in hard ductile layer was more than that in soft interlayered model while crack growth length in hard ductile layer was less than that in soft interlayered model for layer angle of more than 60°. Whereas the shear strength of hard ductile gypsum is more than that of soft brittle gypsum,

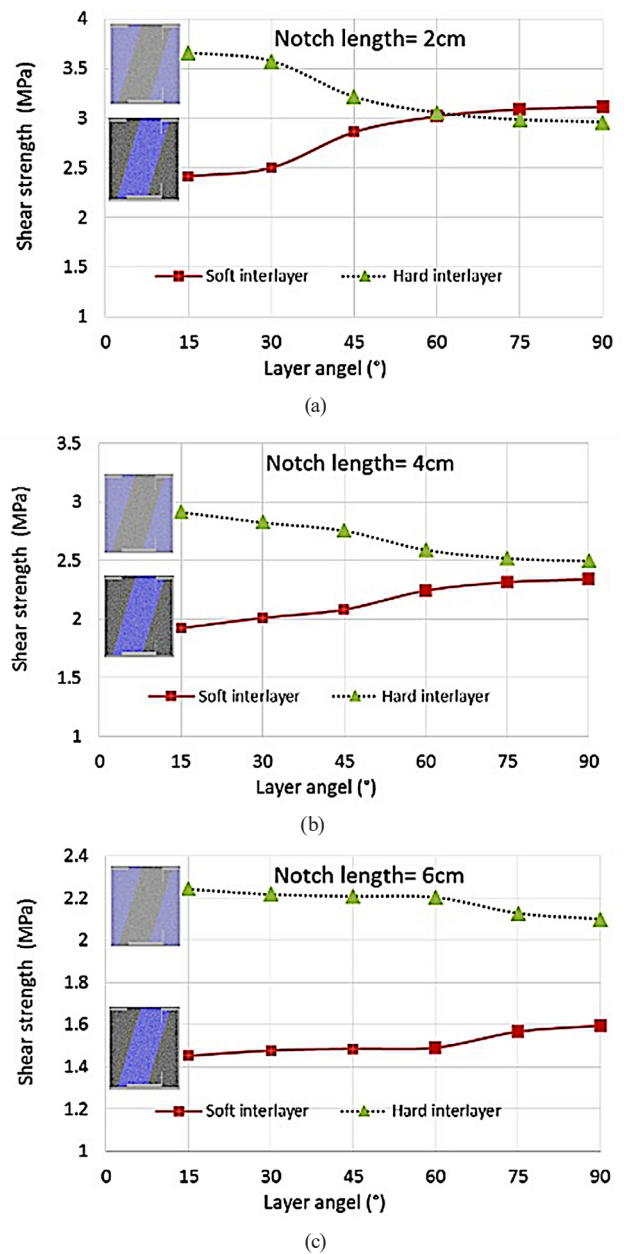


Fig. 8 Effect of layer angle on shear strength for notch length of, (a) 2 cm, (b) 4 cm and (c) 6 cm

therefore shear strength of hard interlayered model was more than that of soft interlayered model for layer angle of less than 60°. When notch lengths were 4 cm and 6 cm, shear strength of hard interlayered model was more than that of soft interlayered model for any layer angle. In these configurations, crack growth length in hard ductile layer was more than that in soft interlayered model. Whereas the shear strength of hard ductile gypsum is more than that of soft brittle gypsum, therefore shear strength of hard interlayered model was more than that of soft interlayered model for any layer angle.

#### 4.6 Influence of notch length on the shear strength

Fig. 9(a) and (b) show the influence of bedding layer angle on the shear strength for soft interlayered model and hard interlayered model, respectively. The results of three notch length were presented in each figure. The shear strength was reduced by enhancing the notch length. This behavior can be attributed to fracture mechanics theory, wherein the stress intensity at the notch tips and the stress interaction between the notch tips is amplified by enhancing the notch length, leading to lower shear strength associated with 6 cm notched models.

By comparison between Fig. 9(a) (for layer angle of  $90^\circ$ ) and Fig. 4(a), it can be concluded that the shear strengths of hard interlayered models are similar to those of physical samples. Also, by comparison between Fig. 9(b) (for layer angle of  $90^\circ$ ) and Fig. 4(b), it can be concluded that the shear strengths of soft interlayered models are similar to those of physical samples.

#### 5 Discussion

There is a close relationship between notch length and shear strength of model. The length of rock bridge was reduced by enhancing the notch length. This leads to enhancing the stress intensity at tip of the notches and increasing the stress interaction between the notches. Therefore, the required energy for crack propagation was decreased and shear strength was decreased, too.

When notch length was 2 cm and layer angle was less than  $60^\circ$ , both shear strength and shear stiffness of hard interlayered model was more than that of soft interlayered model. When layer angle was more than  $60^\circ$ , both shear strength and shear stiffness of soft interlayered model was more than that of hard interlayered model. In other word, when layer angle was less than  $60^\circ$ , crack growth length in hard ductile layer was more than that in soft interlayered model while crack growth length in hard ductile layer was less than that in soft interlayered model for layer angle of more than  $60^\circ$ . Whereas the mechanical properties of hard ductile gypsum are more than that of soft brittle gypsum, therefore both shear strength and shear stiffness of hard interlayered model was more than that of soft interlayered model for layer angle of less than  $60^\circ$ . When notch lengths were 4 cm and 6 cm, both shear strength and shear stiffness of hard interlayered model was more than that of soft interlayered model for any layer angle. In these configurations, crack growth length in hard ductile layer was more than that in soft interlayered model. Whereas the mechanical properties of hard ductile gypsum are more than that

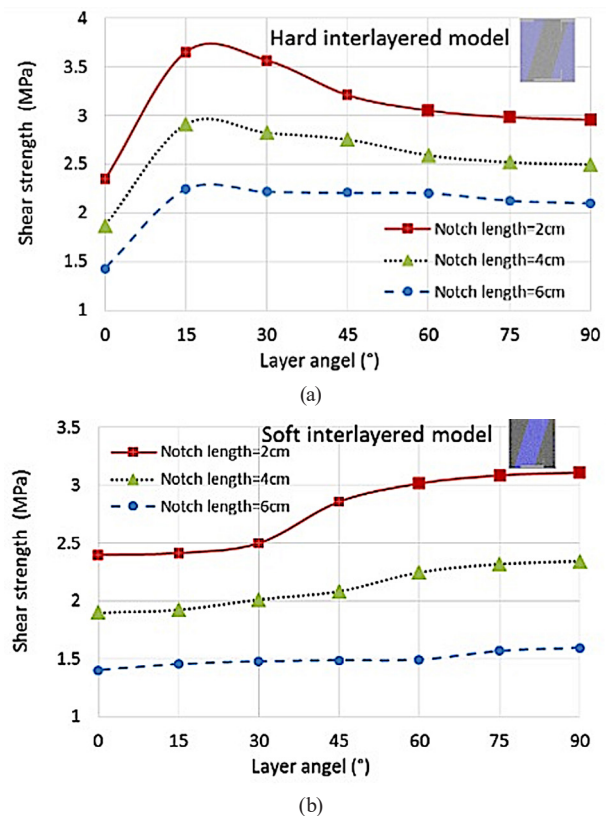


Fig. 9 Effect of bedding angle on the shear strength for, (a) soft interlayer model and (b) hard interlayer model

of soft brittle gypsum, therefore both shear strength and shear stiffness of hard interlayered model was more than that of soft interlayered model for any layer angle. When notch length was 2 cm and layer angle was less than  $60^\circ$ , axial displacement associated to maximum shear stress of hard interlayered model was more than that of soft interlayered model. When layer angle was more than  $60^\circ$ , axial displacement associated to maximum shear stress of soft interlayered model was more than that of hard interlayered model. When notch lengths were 4 cm and 6 cm, axial displacement associated to maximum shear stress of hard interlayered model was more than that of soft interlayered model for any layer angle.

#### 6 Conclusions

In present study, the effect of interlayer mechanical characteristics on the rock shear strength, shear stiffness and failure pattern was studied using experimental test and PFC simulation. Also, the influences of layer angle and notch length on the shear mechanism of notched bedding rock were cleared. The results show that:

- In all configurations, the tensile crack initiates from the notch tip and propagated parallel to the shear loading direction until coalescence with the model boundary.

- Shear displacement related to maximum shear stress was reduced by enhancing the notch length.
- The number of fractures in the soft layer was more than that in the hard layer due to the brittleness effect of soft gypsum.
- The shear strength of the hard interlayered model was decreased by increasing the layer angle while the shear strength of the soft interlayered model was increased by raising the layer angle.
- In all configurations, the angles between micro-cracks and the horizontal axis changed from 75 to 105 degrees.
- In constant notch length, the crack quantities in the soft interlayered model were more than that in the hard interlayered model.

- Failure patterns, shear stiffness, and shear strengths of notched bedding models are similar to those of notched physical samples.

### Acknowledgment

This research was funded by a grant to authors by the vice-president research office of Bu-Ali Sina University, Iran, which is gratefully acknowledged. Also, preparation of testing samples and conducting experiments were undertaken in the Engineering Geological and Geotechnical Laboratory of Bu-Ali Sina University. Therefore, thanks and appreciation for the contributions made in this field.

### References

- [1] Hoek, E. "Fracture of anisotropic rock", *Journal of the South African Institute of Mining and Metallurgy*, 64(10), pp. 501–518, 1964.
- [2] Bidgoli, M. N., Jing, L. "Anisotropy of strength and deformability of fractured rocks", *Journal of Rock Mechanics and Geotechnical Engineering*, 6(2), pp. 156–164, 2014.  
<https://doi.org/10.1016/j.jrmge.2014.01.009>
- [3] Barton, N., Quadros, E. "Anisotropy is everywhere, to see, to measure and to model", *Rock Mechanics and Rock Engineering*, 48, pp. 1323–1339, 2015.  
<https://doi.org/10.1007/s00603-014-0632-7>
- [4] Lee, Y.-K., Pietruszczak, S. "Tensile failure criterion for transversely isotropic rocks", *International Journal of Rock Mechanics and Mining Sciences*, 79, pp. 205–215, 2015.  
<https://doi.org/10.1016/j.ijrmms.2015.08.019>
- [5] Duan, K., Kwok, C. Y. "Discrete element modelling of anisotropic rock under Brazilian test conditions", *International Journal of Rock Mechanics and Mining Sciences*, 78, pp. 46–56, 2015.  
<https://doi.org/10.1016/j.ijrmms.2015.04.023>
- [6] Yang, S.-Q., Yin, P.-F., Zhang, Y.-C., Chen, M., Zhou, X.-P., Jing, H.-W., Zhang, Q.-Y. "Failure behavior and crack evolution mechanism of a non-persistent jointed rock mass containing a circular hole", *International Journal of Rock Mechanics and Mining Sciences*, 114, pp. 101–121, 2019.  
<https://doi.org/10.1016/j.ijrmms.2018.12.017>
- [7] Al-Harathi, A. A. "Effect of planar structures on the anisotropy of Ranyah sandstone, Saudi Arabia", *Engineering Geology*, 50(1–2), pp. 49–57, 1998.  
[https://doi.org/10.1016/S0013-7952\(97\)00081-1](https://doi.org/10.1016/S0013-7952(97)00081-1)
- [8] Ramamurthy, T. "Strength and modulus responses of transversely isotropic rocks", In: Hudson, J. A. (ed.) *Compressive Rock Engineering*, Vol. 1, Pergamon, 1993, pp. 313–329.
- [9] Zhou, X. P., Cheng, H., Feng, Y. F. "An experimental study of crack coalescence behaviour in rock-like materials containing multiple flaws under uniaxial compression", *Rock Mechanics and Rock Engineering*, 47(6), pp. 1961–1986, 2014.  
<https://doi.org/10.1007/s00603-013-0511-7>
- [10] Zhou, Y.-Y., Feng, X.-T., Xu, D.-P., Fan, Q.-X. "Experimental investigation of the mechanical behavior of bedded rocks and its implication for high sidewall caverns", *Rock Mechanics and Rock Engineering*, 49, pp. 3643–3669, 2016.  
<https://doi.org/10.1007/s00603-016-1018-9>
- [11] Shang, J., Duan, K., Gui, Y., Handley, K., Zhao, Z. "Numerical investigation of the direct tensile behaviour of laminated and transversely isotropic rocks containing incipient bedding planes with different strengths", *Computers and Geotechnics*, 104, pp. 373–388, 2018.  
<https://doi.org/10.1016/j.compgeo.2017.11.007>
- [12] Zhang, G.-M., Li, Y.-P., Shi, X.-L., Yang, C.-H., Wang, L.-J. "Research on a model material preparation method for alternate layered rock mass and preliminary experiment", *Yantu Lixue/Rock and Soil Mechanics*, 32, 284–289, 2011.
- [13] Wang, M., Wan, W., Zhao, Y. "Experimental study on crack propagation and the coalescence of rock-like materials with two pre-existing fissures under biaxial compression", *Bulletin of Engineering Geology and the Environment*, 79(6), pp. 3121–3144, 2020.  
<https://doi.org/10.1007/s10064-020-01759-1>
- [14] Geng, J., Chen, W. "Analysis on deformation mechanism of high rock slope of hydropower station under complex hydrogeology", *Microprocessors and Microsystems*, 81, 103733, 2021.  
<https://doi.org/10.1016/j.micpro.2020.103733>
- [15] Yang, S.-Q., Chen, M., Huang, Y.-H., Jing, H.-W., Ranjith, P. G. "An experimental study on fracture evolution mechanism of a non-persistent jointed rock mass with various anchorage effects by DSCM, AE and X-ray CT observations", *International Journal of Rock Mechanics and Mining Sciences*, 134, 104469, 2020.  
<https://doi.org/10.1016/j.ijrmms.2020.104469>
- [16] Brady, B. H. G., Brown, E. T. "Rock Mechanics: For Underground Mining", Springer, 2006. ISBN: 978-1-4020-2064-3  
<https://doi.org/10.1007/978-1-4020-2116-9>
- [17] Sagong, M., Bobet, A. "Coalescence of multiple flaws in a rock-model material in uniaxial compression", *International Journal of Rock Mechanics and Mining Sciences*, 39(2), pp. 229–241, 2002.  
[https://doi.org/10.1016/S1365-1609\(02\)00027-8](https://doi.org/10.1016/S1365-1609(02)00027-8)

- [18] Asadizadeh, M., Moosavi, M., Hossaini, M. F., Masoumi, H. "Shear strength and cracking process of non-persistent jointed rocks: an extensive experimental investigation", *Rock Mechanics and Rock Engineering*, 51(2), pp. 415–428, 2018.  
<https://doi.org/10.1007/s00603-017-1328-6>
- [19] Asadizadeh, M., Hossaini, M. F., Moosavi, M., Masoumi, H., Ranjith, P. G. "Mechanical characterization of jointed rock-like material with non-persistent rough joints subjected to uniaxial compression, *Engineering Geology*", 260, 105224, 2019.  
<https://doi.org/10.1016/j.enggeo.2019.105224>
- [20] Prudencio, M., Van Sint Jan, M. "Strength and failure modes of rock mass models with non-persistent joints", *International Journal of Rock Mechanics and Mining Sciences*, 44(6), pp. 890–902, 2007.  
<https://doi.org/10.1016/j.ijrmms.2007.01.005>
- [21] Yang, S.-Q. "Crack coalescence behavior of brittle sandstone samples containing two coplanar fissures in the process of deformation failure", *Engineering Fracture Mechanics*, 78, pp. 3059–3081, 2011.  
<https://doi.org/10.1016/j.engfracmech.2011.09.002>
- [22] Yang, X.-X., Qiao, W.-G. "Numerical investigation of the shear behavior of granite materials containing discontinuous joints by utilizing the flat-joint model", *Computer and Geotechnics*, 104, pp. 69–80, 2018.  
<https://doi.org/10.1016/j.compgeo.2018.08.014>
- [23] Liu, B., Zhou, Y., Gao, Y.-T., Xu, C. "Experimental and numerical study on crack development characteristics between two cavities in rock-like material under uniaxial compression", *Theoretical and Applied Fracture Mechanics*, 109(3), 102755, 2020.  
<https://doi.org/10.1016/j.tafmec.2020.102755>
- [24] Zhao, Y., Zhang, L., Wang, W., Pu, C., Wan, W., Tang, J. "Cracking and stress–strain behavior of rock-like material containing two flaws under uniaxial compression", *Rock Mechanics and Rock Engineering*, 49(7), pp. 2665–2687, 2016.  
<https://doi.org/10.1007/s00603-016-0932-1>
- [25] Chen, X., Liao, Z., Peng, X. "Deformability characteristics of jointed rock masses under uniaxial compression", *International Journal of Mining Science and Technology*, 22(2), pp. 213–221, 2012.  
<https://doi.org/10.1016/j.ijmst.2011.08.012>
- [26] Kulatilake, P. H. S. W., Malama, B., Wang, J. "Physical and particle flow modeling of jointed rock block behavior under uniaxial loading", *International Journal of Rock Mechanics and Mining Sciences*, 38, pp. 641–57, 2001.  
[https://doi.org/10.1016/S1365-1609\(01\)00025-9](https://doi.org/10.1016/S1365-1609(01)00025-9)
- [27] Tien, Y. M., Kuo, M. C., Juang, C. H. "An experimental investigation of the failure mechanism of simulated transversely isotropic rocks", *International Journal of Rock Mechanics and Mining Sciences*, 43, pp. 1163–81, 2006.  
<https://doi.org/10.1016/j.ijrmms.2006.03.011>
- [28] Gatelier, N., Pellet, F., Lorent, B. "Mechanical damage of an anisotropic porous rock in cyclic triaxial tests", *International Journal of Rock Mechanics and Mining Sciences*, 39(3), pp. 335–354, 2002.  
[https://doi.org/10.1016/S1365-1609\(02\)00029-1](https://doi.org/10.1016/S1365-1609(02)00029-1)
- [29] Zhou, X., Wang, Y., Xu, X. "Numerical simulation of initiation, propagation and coalescence of cracks using the non-ordinary state-based peridynamics", *International Journal of Fracture*, 201(2), pp. 213–234, 2016.  
<https://doi.org/10.1007/s10704-016-0126-6>
- [30] Shang, J., West, L. J., Hencher, S. R., Zhao, Z. "Geological discontinuity persistence: Implications and quantification", *Engineering Geology*, 241, pp. 41–54, 2018.  
<https://doi.org/10.1016/j.enggeo.2018.05.010>
- [31] Chiu, C.-C., Wang, T.-T., Weng, M.-C., Huang, T.-H. "Modelling the anisotropic behavior of jointed rock mass using a modified smooth-joint model", *International Journal of Rock Mechanics and Mining Sciences*, 62, pp. 14–22, 2013.  
<https://doi.org/10.1016/j.ijrmms.2013.03.011>
- [32] Zhao, B., Liu, Y., Huang, T., Wang, X. "Experimental Study on Strength and Deformation Characteristics of Rock–Concrete Composite Specimens Under Compressive Condition", *Geotechnical and Geological Engineering*, 37, pp. 2693–2706, 2019.  
<https://doi.org/10.1007/s10706-018-00787-9>
- [33] Han, Z., Li, D., Zhou, T., Zhu, Q., Ranjith, P. G. "Experimental study of stress wave propagation and energy characteristics across rock specimens containing cemented mortar joint with various thicknesses", *International Journal of Rock Mechanics and Mining Sciences*, 131, 104352, 2020.  
<https://doi.org/10.1016/j.ijrmms.2020.104352>
- [34] Wen, S., Zhang, C., Chang, Y., Hu, P. "Dynamic compression characteristics of layered rock mass of significant strength changes in adjacent layers", *Journal of Rock Mechanics and Geotechnical Engineering*, 12(2), pp. 353–365, 2020.  
<https://doi.org/10.1016/j.jrmge.2019.09.003>
- [35] Yaylaci, M., Yaylaci, E. U., Ozdemir, M. E., Ozturk, Ş., Sesli, H. "Vibration and buckling analyses of FGM beam with edge crack: Finite element and multilayer perceptron methods", *Steel and Composite Structures*, 46(4), pp. 565–575, 2023.  
<https://doi.org/10.12989/scs.2023.46.4.565>
- [36] Özdemir, M. E., Yaylac, M. "Research of the impact of material and flow properties on fluid-structure interaction in cage systems", *Wind and Structure*, 36(1), pp. 31–40, 2023.  
<https://doi.org/10.12989/was.2023.36.1.031>
- [37] Yaylaci, M., Şabano, B. Ş., Özdemir, M. E., Birinci, A. "Solving the contact problem of functionally graded layers resting on a HP and pressed with a uniformly distributed load by analytical and numerical methods", *Structural Engineering and Mechanics*, 82(3), pp. 401–416, 2022.  
<https://doi.org/10.12989/sem.2022.82.3.401>
- [38] Potyondy, D. O., Cundall, P. A. "A bonded-particle model for rock", *International Journal of Rock Mechanics and Mining Sciences*, 41, pp. 1329–1364, 2004.  
<https://doi.org/10.1016/j.ijrmms.2004.09.011>
- [39] Potyondy, D. O. "The bonded-particle model as a tool for rock mechanics research and application: Current trends and future directions", *Geosystem Engineering*, 18(1), pp. 1–28, 2015.  
<https://doi.org/10.1080/12269328.2014.998346>
- [40] Ivars, D. M., Potyondy, D. O., Pierce, M., Cundall, P. A. "The smooth-joint contact model", presented at the 8th World Congress on Computational Mechanics (WCCM8) 5th European Congress on Computational Methods in Applied Sciences and Engineering (ECCOMAS 2008), Venice, Italy, 30 June–5 July, 2008.